JOURNAL OF GEOPHYSICAL RESEARCH, VOL. 111, D24108, doi:10.1029/2006JD007354, 2006

Lidar temperature measurements of gravity waves over Kühlungsborn (54°N) from 1 to 105 km: A winter-summer comparison

M. Rauthe,[1] M. Gerding,[1] J. Höffner,[1] and F.-J. Lübken[1]

Received 30 March 2006; revised 18 July 2006; accepted 10 August 2006; published 21 December 2006.

[1] Since August 2002, temperature measurements from 1 to 105 km are performed at the Leibniz Institute of Atmospheric Physics in Kühlungsborn (54°N) with a combination of different lidars. Results from 14 nights in winter and 31 in summer are presented. Nightly mean profiles and fluctuations with a temporal and vertical resolution of 15 min and 1 km, respectively, are derived. In both seasons, wave energy propagates upward (phase propagates downward) with vertical phase speeds of −0.25 to −1.9 m/s. Phase speeds are generally larger in the mesosphere compared to the stratosphere because of decreasing static stability. Wave periods are found in the entire range of 1–8 hours (given by experimental constraints) with no preference for particular periods. The observed vertical wavelengths cover the entire instrumental range of 5–50 km, but the majority lies below 22 km in both seasons. In single nights, a few waves (up to three) dominate the wave spectrum and represent 45–65% of the entire variability. Wave amplitudes generally increase with altitude with a scale height of ∼18–22 km, i.e., less than expected (14 km) for propagation conserving momentum flux density. The gravity wave energy loss changes with altitude and is different in both seasons. Local fluctuation minima (“nodes”) are often observed, frequently colocated with convective instabilities. Temperature fluctuations are generally smaller in summer compared to winter (maximum values are 10 and 25 K, respectively). Applying gravity wave polarization relations to the mean winter and summer lidar temperature profiles, the difference of fluctuations is basically determined by the background conditions, especially at ∼60–80 km.

Citation: Rauthe, M., M. Gerding, J. Höffner, and F.-J. Lübken (2006), Lidar temperature measurements of gravity waves over Kühlungsborn (54°N) from 1 to 105 km: A winter-summer comparison, *J. Geophys. Res.*, *111*, D24108, doi:10.1029/2006JD007354.

1. Introduction

[2] Atmospheric gravity waves have been the subject of intense research activity in recent years because of their tremendous importance for atmospheric circulation, structure, and variability (see review by *Fritts and Alexander* [2003] and references therein). Gravity waves contribute to turbulence and mixing, and influence the mean circulation and the thermal structure of the middle and upper atmosphere [*Lindzen*, 1981; *Holton*, 1982; *Manzini and McFarlane*, 1998; *Holton and Alexander*, 2000]. It has been widely recognized that gravity waves play a special role in the entire spectrum of atmospheric waves [e.g., *Fritts and Alexander*, 2003].

[3] A number of experimental campaigns and long-term studies have been performed to study characteristics and effects of gravity waves in the lower, middle, and upper atmosphere [e.g., *Meek et al.*, 1985; *Dao et al.*, 1995; *Eckermann et al.*, 1995; *Hertzog et al.*, 2002; *Dörnbrack et al.*, 2002; *Schöch et al.*, 2004]. So far, however, there have been only few techniques which allow to observe gravity waves with small vertical and horizontal scales and short periods. Satellites promise a global coverage but cannot adequately resolve small vertical and horizontal scales [e.g., *Fetzer and Gille*, 1994; *Preusse et al.*, 2002; *Ern et al.*, 2004]. Radiosondes and rocket soundings can provide information on short vertical scales but in a limited height region and on snapshot basis only [e.g., *Allen and Vincent*, 1995; *Vincent and Alexander*, 2000; *Eckermann et al.*, 1995; *Rapp et al.*, 2004]. Radars do not cover the upper stratosphere and lower mesosphere since the backscatter signal is too weak [e.g., *Nakamura et al.*, 1996; *Dalin et al.*, 2004; *Serafimovich et al.*, 2005]. Airglow imagers produce data with high temporal and horizontal resolution, but the gravity wave field can only be observed at single altitudes [e.g., *Hecht et al.*, 2004]. Lidar is the only technique which allows quasi-permanent observations from the troposphere up to the lower thermosphere with an appropriate time and height resolution for observation of medium and low-frequency gravity waves. Several lidar results on gravity waves have been published but most of them cover only a rather small altitude region given by the specific instruments

[1] Leibniz-Institut für Atmosphärenphysik an der Universität Rostock, Kühlungsborn, Germany.

0148-0227/06/2006JD007354$09.00

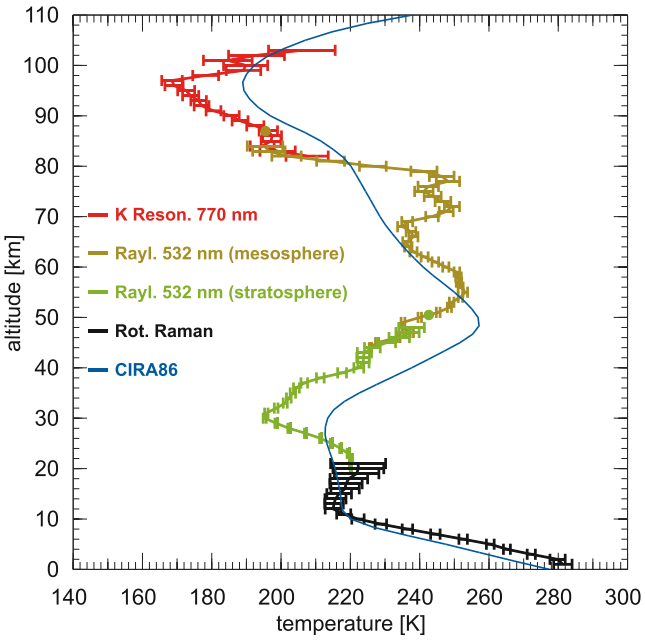

Figure 1. Temperature profile obtained from a combination of different lidar techniques measured on 12 November 2003, 1945–2045 UT, above Kühlungsborn. The dots show the start values for the Rayleigh integrations; the blue line is the CIRA86 reference atmosphere.

available [*Gardner and Voelz*, 1987; *Gardner et al.*, 1989; *Wilson et al.*, 1991a, 1991b; *Sica and Russell*, 1999]. None of these studies covers the entire height range relevant for gravity wave studies, namely from their source (troposphere) to their main dissipation region (mesosphere). Only very few case studies of gravity waves from the troposphere to the upper mesosphere are available [*Dao et al.*, 1995; *Sica et al.*, 1995; *Williams et al.*, 2004].

[4] In this paper we present lidar temperature measurements of gravity waves from the troposphere up to the lower thermosphere (~105 km) representing typical winter and summer conditions. We concentrate on nighttime observations because at daytime the S/N ratio (signal-to-noise ratio) is not high enough to calculate temperatures in the entire altitude range with sufficient temporal resolution. We use data from two different lidars, namely a Rayleigh-Mie-Raman lidar (RMR lidar) at 532 nm and a potassium resonance lidar at 770 nm, which are operated at the Leibniz Institute of Atmospheric Physics (IAP) in Kühlungsborn, Germany (54°N, 12°E) [*Alpers et al.*, 2004]. These lidars are capable of acquiring night mean temperature profiles and the corresponding variations during the night with a height resolution of ~0.2–1 km (depending on altitude) and a temporal resolution of up to 5 min. In this paper we use a temporal and vertical resolution of 15 min and 1 km, respectively, to cover the largest possible altitude range from 1–105 km.

[5] In section 2 and 3 we describe the observational methods and present examples of gravity wave measurements over Kühlungsborn in winter and summer. In section 4 the entire data set for winter and summer is analyzed in terms of gravity waves (total of 45 nights). In section 5 and 6 we discuss the results, and present our conclusions.

2. Observation Methods

2.1. Lidar Systems

[6] Lidar observations are carried out at night with a potassium resonance lidar and a RMR lidar at the IAP in Kühlungsborn since August 2002. Depending on altitude we use three different methods for temperature measurements (more details are described by *Alpers et al.* [2004]):

[7] 1. A tunable narrowband potassium resonance lidar yields temperatures from ~80 to 105 km from the spectral broadening of the 770 nm K-D_1 resonance line [*von Zahn and Höffner*, 1996]. This system has full daylight capability [*Fricke-Begemann et al.*, 2002; *Fricke-Begemann and Höffner*, 2005], which, however, is not used in this study because the other techniques (see below) are restricted to nighttime.

[8] 2. Temperatures between about 22 and 90 km are measured by a RMR lidar. The Rayleigh backscatter at 532 nm provides relative atmospheric density profiles. Relative density profiles are then converted to temperature profiles assuming hydrostatic equilibrium. The required temperature value at the top of the profile is given by the potassium lidar. In this way temperature profiles are obtained from 90 km down to 45 km. Lower altitudes are covered by a second separate channel (22–50 km) with smaller sensitivity to deal with the large dynamical range. In the height range ~22–32 km an altitude-dependent correction on the order of 1–5 K is performed because of signal contamination from stratospheric aerosols (for details, see *Alpers et al.* [2004] and *Gerding et al.* [2004]). This correction cannot be applied below 22 km because of the high variability of the aerosols in the troposphere and lower stratosphere.

[9] 3. The rotational Raman backscatter in two narrow wavelength ranges (529.08 ± 0.51 nm and 530.38 ± 0.47 nm) are also measured by the RMR lidar and gives temperature profiles in the lower stratosphere and troposphere (~1–25 km) [e.g., *Vaughan et al.*, 1993; *Alpers et al.*, 2004].

[10] Figure 1 shows an example of a temperature profile (integrated over 1 hour) calculated with the techniques presented above. Several local maxima and minima are present in Figure 1. These temperature fluctuations were the first indication of wave signatures in our measurements. The statistical uncertainty of these temperature profiles is typically 1.5–2.5 K and nowhere exceeds 10 K (see Figure 1). The backscatter signals of the Rayleigh and Raman channel are proportional to $\rho(z)/z^2$ (ρ = air density, z = altitude). This implies that the rotational Raman signal from 20 km is about a factor of 20 (400) weaker than from 10 km (3 km). Therefore the statistical uncertainty between 10 and 20 km increases rapidly with height (see Figure 1). Above 22 km we use the elastic Rayleigh signal, which has a factor of $\sim 10^4$ larger backscatter cross section compared to rotational Raman and therefore much smaller statistical errors (see Figure 1). Altogether, the statistical uncertainties above 22 km are smaller than typical temperature fluctuations with the exception of 38–45 km, where both are of same order of magnitude. We construct continuous temperature profiles using the technique with the smallest

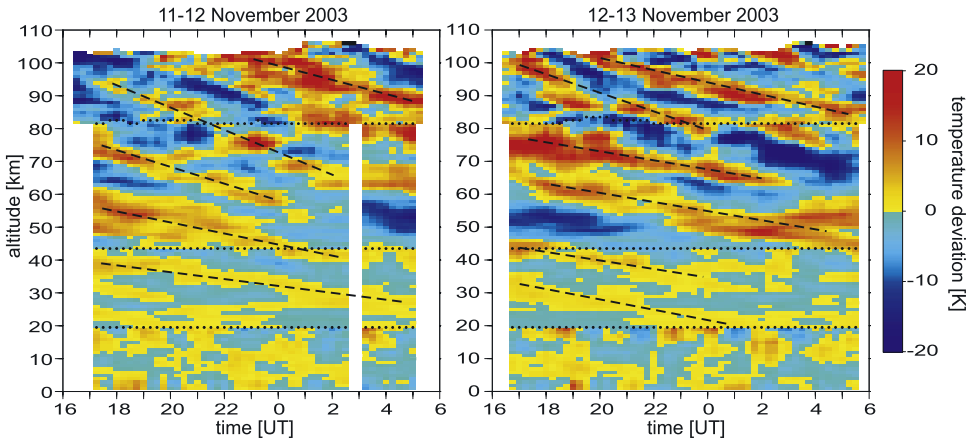

Figure 2. Temperature deviations from the nightly mean for two consecutive nights (11–12 and 12–13 November 2003). The dashed lines indicate the phase propagation. The dotted lines indicate the transition heights between different measurement methods. The gap in the RMR data at ~0300 UT (left plot) is due to technical reasons.

statistical uncertainty in overlapping heights. As can be seen in Figure 1 the difference between the observed temperature and the climatological mean (represented by CIRA86 reference atmosphere [*Fleming et al.*, 1990]) exceeds 20 K at some altitudes. The observed profile demonstrates the advantage of using locally observed, time-dependent temperatures for initialization of Rayleigh temperature retrieval. For example, the use of mean CIRA86 temperatures instead of actual measurements would introduce a time-dependent error of nearly 20 K in the upper part of the Rayleigh temperature profile.

[11] We smooth the raw profiles applying an altitude-dependent filter length (0.6 and 3 km at 40 km and 80 km, respectively) and a running mean over 1 hour with 15 min time shift. Finally, the data are binned into 1 km altitude bins. This procedure provides continuous profiles with a good trade-off between statistical uncertainty and temperature fluctuation.

2.2. Gravity Wave Parameters

[12] To describe the gravity wave activity we calculate the following altitude-dependent parameters from the lidar measurements: temperature deviations from nightly mean (ΔT), their maximum (ΔT_{max}), and their mean ($\overline{|\Delta T|}$). In addition to temperature fluctuations, we determine vertical phase speeds, wave periods, and vertical wavelengths. Note that phase speeds and periods are obtained relative to a ground-based station (intrinsic values may be different because of a Doppler shift). We calculate the vertical phase speeds ($c_{\phi,z}$) from the slope of lines of constant phase in the time-height plane. Periods (P) are calculated by Fourier transformation of single time series, and vertical wavelengths (λ_z) are calculated by wavelet analyses of single altitude profiles. We use a Morlet wavelet of fifth order which is a good approach for many geophysical applications [*Torrence and Compo*, 1998]. The altitude range and resolution determine the maximum and minimum detectable vertical wavelengths. The measurement duration and the time resolution determine the range of wave periods. Taking into account the lidar capabilities varying with height and season, we derive vertical wavelengths with the wavelet analyses in the range 5–50 km for winter and summer. Periods in the range 1.5–12 hours for winter and 1.5–3.5 hours for summer are resolved by our instrumental technique.

3. Examples for Summer and Winter Seasons

3.1. Observations on 11–12 and 12–13 November 2003

[13] In this section we present measurements from two consecutive nights in winter. Temperature deviations from the mean on 11–12 November and 12–13 November 2003 are shown in Figure 2, covering more than 12 hours each. Coherent wave structures are clearly visible in both nights. The phase progresses downward with time indicating an upward transport of energy. The phase speed varies between −0.25 and −0.75 m/s (see Figure 2 dashed lines). Larger (absolute) values occur in the mesosphere compared to the stratosphere.

[14] The magnitude of the fluctuations is similar in both nights (see Table 1) and is also typical for the season (cf. section 4.1). Figure 3 shows individual profiles of temperature fluctuations for both nights. The statistical uncertainties as described in section 2.1 are also shown. In the height ranges 10–22 km and 38–45 km the statistical uncertainties are of the same order as the temperature

Table 1. Mean Fluctuations for Different Altitude Ranges for the Two Winter Cases and for the Summer Case in 2003[a]

	$\overline{\lvert\Delta T\rvert}$, K		
Altitude, km	11–12 Nov	12–13 Nov	13–14 Jun
20–30	1.0 (0.7)	0.8 (0.4)	0.3
30–40	1.6 (1.1)	1.3 (0.8)	1.3
40–50	2.8 (2.3)	4.4 (2.3)	1.2
50–60	4.6 (2.3)	5.2 (2.7)	0.8
60–70	4.0 (3.5)	5.9 (4.5)	1.4
70–80	5.3 (4.3)	8.9 (4.1)	3.3
80–90	5.6 (4.1)	6.1 (5.4)	2.5
90–100	7.0 (5.2)	6.2 (5.5)	5.4

[a]The values in parentheses give the corresponding fluctuation in hours for the case when the analysis is restricted to the length of the summer case (3.5 hours).

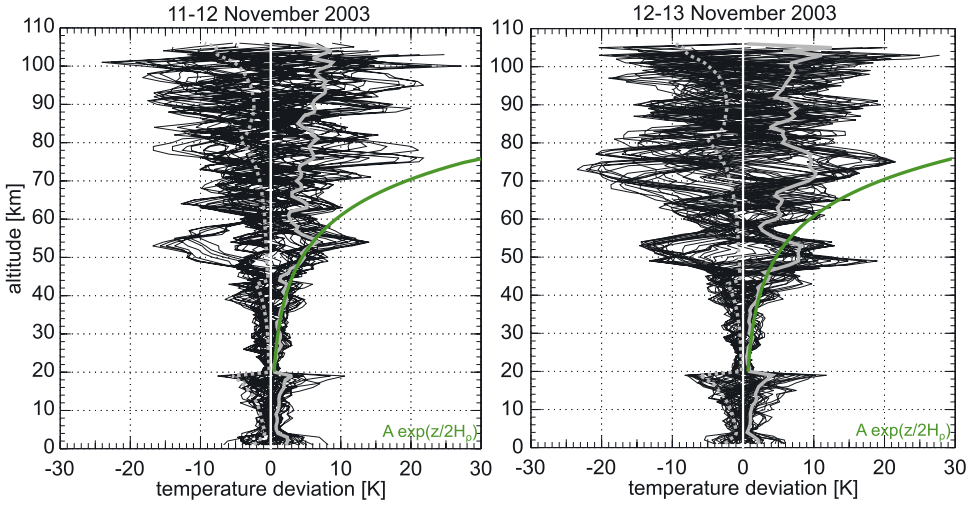

Figure 3. Individual temperature deviation profiles on 11–12 and 12–13 November 2003 (each profile with 1 hour integration time and time shift of 15 min). In addition, the mean statistical uncertainties of the measurements (gray dashed line) and the mean fluctuations at every altitude (gray solid line) are shown. The green line shows an exponential growth $\sim$exp ($z/2H_\rho$) with a constant density scale height H_ρ = 7 km.

fluctuations. We therefore hesitate to determine wave amplitudes at these altitudes but still use the data for analyses of periods and vertical wavelengths. As can be seen in Figure 3 fluctuations generally increase with altitude above 22 km, however, less than expected from conservation of momentum flux density and decreasing air density (cf. the green line with the fluctuations). The maximum fluctuations (ΔT_{max}) increase from 0.5–1.5 K at 20 km to 10–20 K in the mesosphere. According to $\sim$exp ($z/2H_\rho$) with the density scale height H_ρ = 7 km [*Fritts and Alexander*, 2003] the amplitude of a vertically propagating, unsaturated gravity wave with an amplitude of 0.5 K at 20 km would increase to 9 K and 36 K at 60 and 80 km, respectively. We know that this approximation for "undisturbed" propagation is an oversimplification neglecting the effect of the changing temperature gradient (Brunt-Väisälä frequency), the background wind changes and the saturation of waves. These will be discussed in detail in section 5.2. Additionally, it is obvious from Figure 3 that the fluctuations do not grow monotonically with height but show rather strong decrease at certain altitudes. In the following we will refer to these altitudes as ("nodes"). In the first night a "node" is present at $\sim$60 km and a weaker one at $\sim$86 km. In the second night a "node" is observed at 57 km and weaker ones at 84 and 93 km. Beside these "nodes" the maximum temperature deviations are nearly constant with altitude in the mesosphere.

[15] We have performed Fourier analyses of the temperature fluctuations time series (not shown) and find several wave periods between 1.5 and 8 hours with a very weak preference for longer periods (>6 hours) at all altitudes between 22 and 100 km. There is no significant difference between both nights. To investigate vertical wavelengths, a wavelet spectrum is calculated for every single profile. Figure 4 shows the average spectrum of these morlet transforms for each night. We are careful with the interpretation of the results outside of the triangle (the so-called "cone of influence") because edge effects exist there (the amplitudes are underestimated and the resolution is reduced in these areas) [*Torrence and Compo*, 1998]. We determine the local maxima of the spectrum at every altitude (pluses in Figure 4) and distinguish two separate wavelengths by requiring that the amplitude has to decrease by more than 10% between each maximum. This procedure results in up to three maxima at each altitude. Dominant vertical wavelengths with a range of 11–18 km are observed for the entire altitude range in both nights. Amplitudes are generally somewhat smaller in the first night than in the second. While there is only one dominating vertical wavelength at any given altitude in the first night, two wavelengths are clearly detected between 40 and 70 km in the second night. We have determined the contribution of the dominating wave modes to the total fluctuations by including the power spectrum density. After digitization of artificial waves with a resolution comparable to our measurements the broadening of the wavelength spectrum has been analyzed. The full width at half maximum of such a single wave in the power spectrum was found to be about $\pm 0.2\ \lambda_z$. We now calculate the power fraction of the dominating wave modes ($\lambda_z \pm 0.2\ \lambda_z$) compared to the total power in the altitude range 40–60 km. In the first and second night the dominating modes represent 47% and 63% of the total variability, respectively.

3.2. Observations on 13–14 June 2003

[16] In Figure 5a we show temperature fluctuations for a summer night (13–14 June 2003). Here the measurements cover only 3.5 hours (2145–0115 UT) because of the much shorter time of darkness in summer at our site. Wave structures are clearly visible above 35 km. The ground-based vertical phase speeds are in the range of -1.0 to -1.9 m/s (dashed lines in Figure 5a) and thus larger (in absolute magnitude) than in winter. Similar to the winter cases the phase speeds are larger in the mesosphere compared to the stratosphere.

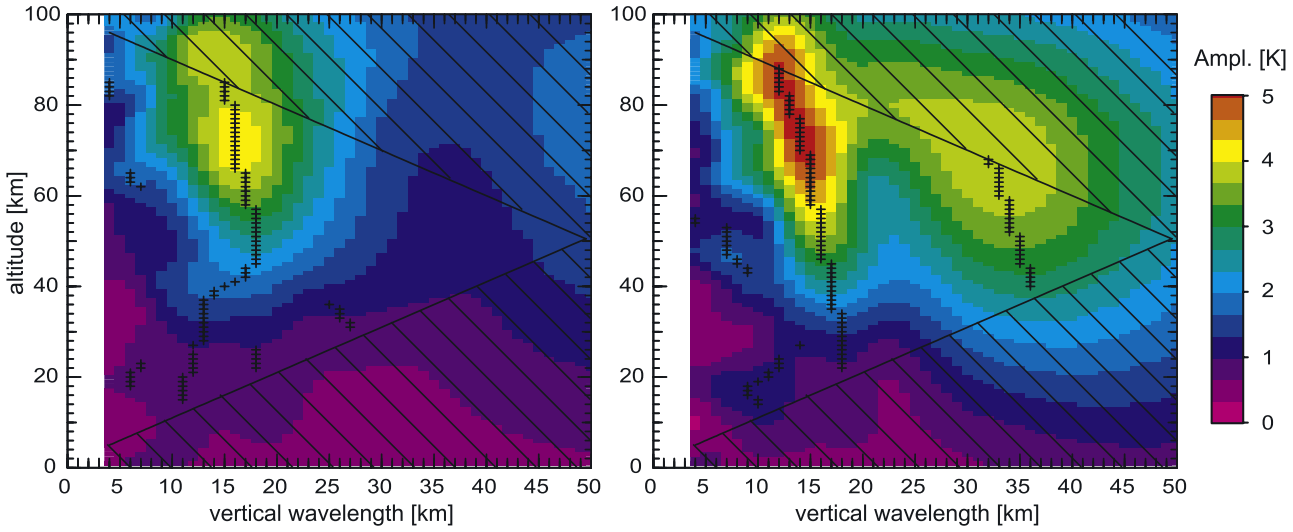

Figure 4. Mean wavelet spectrum of vertical wavelengths for the temperature profiles shown in Figure 2 (11–12 and 12–13 November 2003). Pluses indicate local amplitude maxima. The hatched area indicates the "cone of influence."

[17] The temperature deviation profiles are presented in Figure 5b. They are typical for the summer season (cf. section 4.1) and increasing only moderately between 22 and 70 km from 0.5 K to 3 K. Above 70 km the fluctuations increase rapidly to ~10 K at 95 km. The fluctuations are much smaller than in winter at all altitudes (see also Table 1). To determine the increase with altitude quantitatively we have fitted an exponential function $\exp(z/2H_E)$ to the fluctuations shown in Figure 5b. We find H_E ~11 km between 22 and 80 km (magenta line in Figure 5b) which is significantly larger than expected for undisturbed propagation with the density scale height ($H_\rho \sim 7$ km). This indicates that some nonconservative mechanisms (for example wave breaking or saturation) must have been present. We have not performed this procedure for winter cases because of the large variability of fluctuations and the strong "nodes." Even if the "nodes" are not so prominent and strong as in winter they are also visible in Figure 5b (e.g., at 54 and 82 km.)

[18] A frequency analysis to determine wave periods is not advisable for summer because the maximum detectable period is only 3.5 hours which is too small for a meaningful

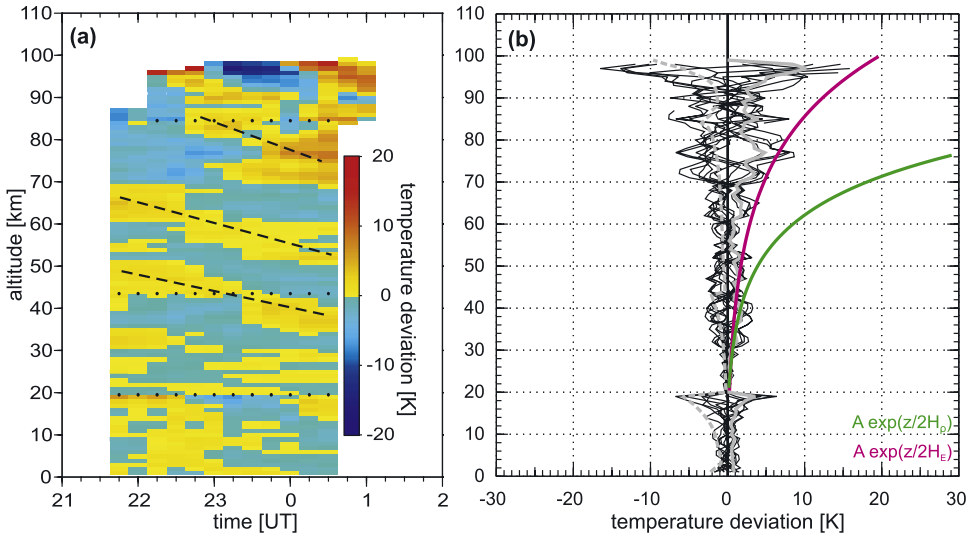

Figure 5. (a) Temperature deviations from the nightly mean for the measurements on 13–14 June 2003. The dashed lines indicate the phase propagation. The dotted lines indicate the transition heights between the different measurement methods. (b) Individual temperature deviation profiles on 13–14 June 2003. In addition, the mean statistical uncertainties of the measurements (gray dashed line) and the mean fluctuations at every altitude (gray solid line) are shown. The green line shows an exponential growth ~exp ($z/2H_\rho$) with a constant density scale height H_ρ = 7 km. The magenta line shows a fit of an exponential growth ~exp ($z/2H_E$) with H_E = 11 km.

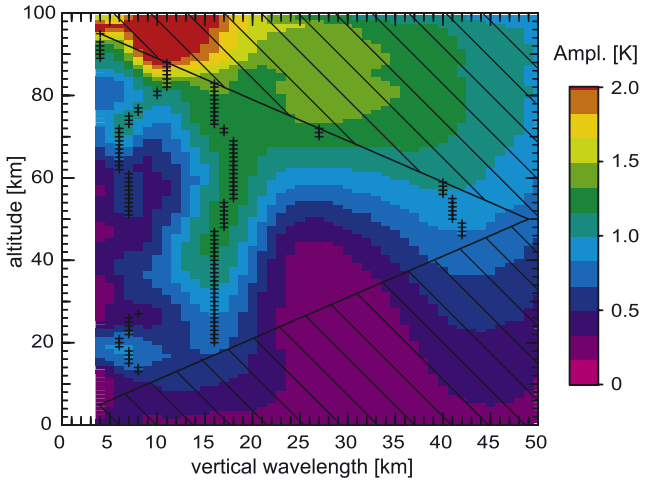

Figure 6. Mean wavelet spectrum of vertical wavelengths for the temperature profiles shown in Figure 5a (13–14 June 2003). Pluses indicate local amplitude maxima. The hatched area indicates the "cone of influence."

interpretation. A wavelet analysis reveals dominating vertical wavelengths of 16–18 km at all altitudes and additional contributions with ~40 km at altitudes of 40–60 km (see Figure 6). Furthermore, vertical wavelengths of less than 10 km are found at all altitudes outside the 30 to 50 km range. The wavelengths are therefore similar to winter, but the amplitudes are smaller by almost a factor of two. At about 50 km altitude the two dominating waves explain about 62% of the total variability.

4. Results From All Summer and Winter Measurements

[19] In the two following subsections we extend our analysis to all available data sets with a duration larger than 3 hours for winter (November, December, January) and summer (June and July). In total 31 summer and 14 winter nights are available from the years 2002–2005. As will be shown in the following the full data set confirms the results presented in the preceding sections. This includes intraseasonal differences and similarities.

4.1. Variability of the Mean Amplitudes

[20] In Figure 7 we show mean fluctuations of all individual nights for summer and winter (cf. the grey solid lines in Figures 3 and 5b). We also determine the mean of the fluctuations at all altitudes and their standard deviations. For this purpose we limit the data evaluation to durations of 3–5 hours to get a comparable data set in winter and summer (as mentioned before, summer measurements are generally shorter because of shorter nighttime conditions). Furthermore, we smooth the data applying a Hanning filter with a width of ±5 km which reduces the influence of the "nodes" on the mean profiles. We have excluded the altitude ranges below 20 km and 38–45 km from this analysis since the statistical uncertainty at these heights is comparable to the fluctuations (see section 2.1). In the range 38–45 km we have linearly interpolated the mean and the standard deviation for further analyses. As can be seen from Figure 7 the mean fluctuations are generally larger in winter compared to summer. In the mesosphere we find typical fluctuations of, e.g., 3 and 5.5 K (winter) and 1.2 and 3 K (summer) at 60 and 80 km, respectively. In summer the fluctuations increase rapidly above ~85 km. Note that profiles from different nights are more similar in summer than in winter; that is, the standard deviations are smaller in summer (red bars in Figure 7). A comparison of the 3.5-hour values in Table 1 and the seasonal means demonstrates that the presented winter and summer examples in sections 3.1 and 3.2 are typical for the gravity wave activity in each season.

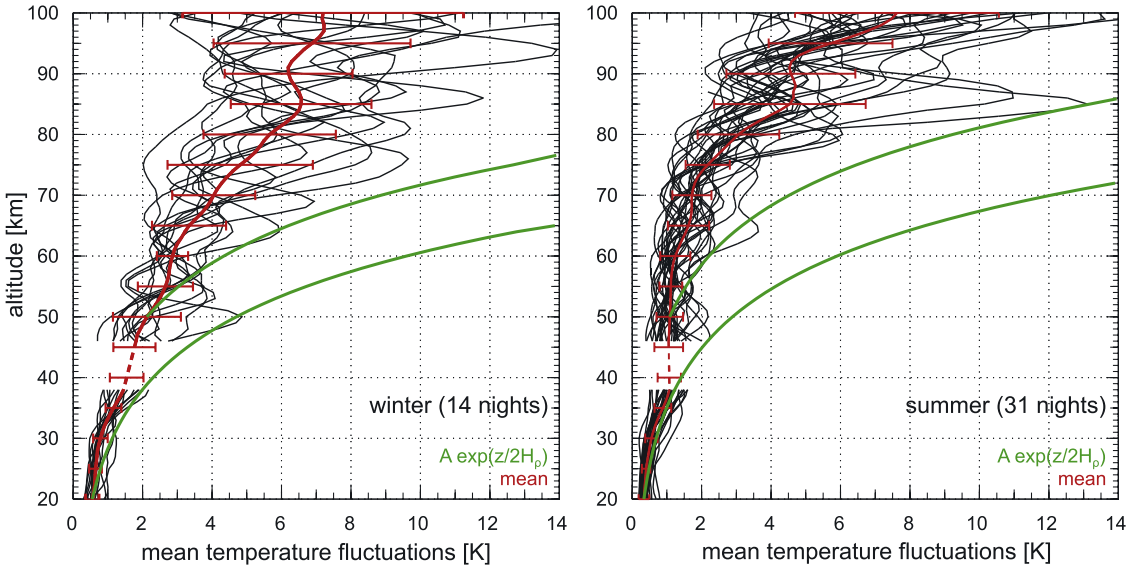

Figure 7. Mean temperature fluctuations of every night for (left) 14 winter and (right) 31 summer measurements. The red line and the bars indicate the mean of all nights and the standard deviation, respectively. The green line shows an exponential growth ~exp ($z/2H_\rho$) with a constant H_ρ = 7 km. Note the interpolation between 38 and 45 km (see text for details).

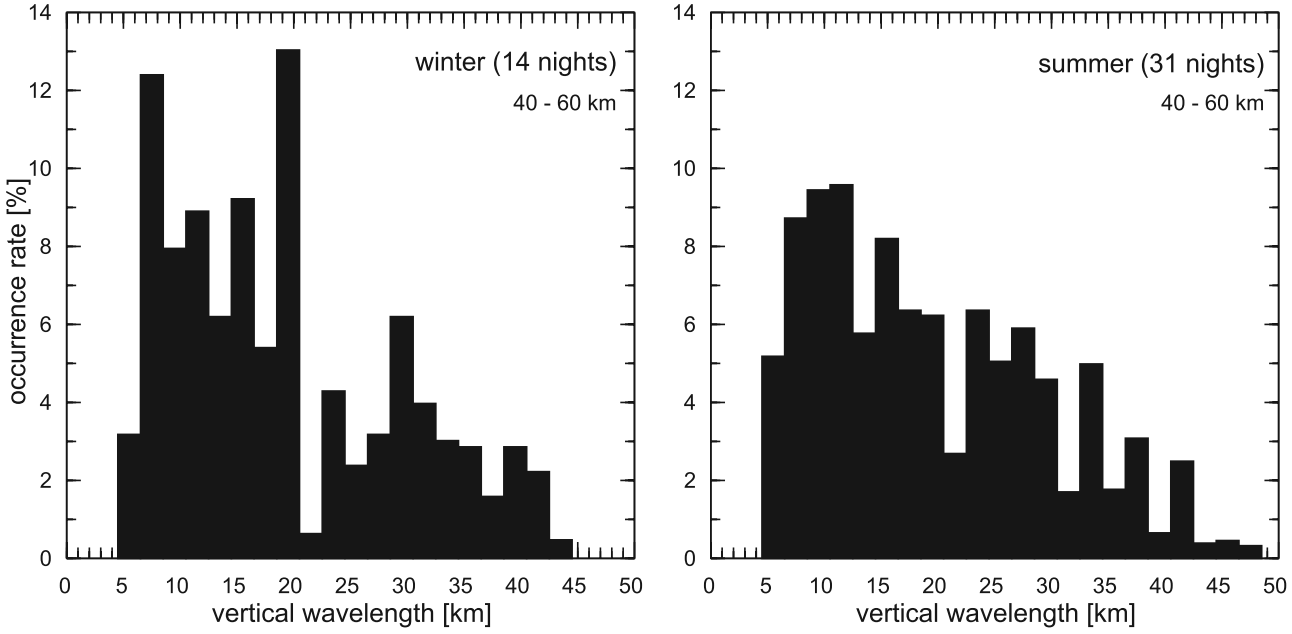

Figure 8. Distribution of dominating vertical wavelengths for (left) 14 winter and (right) 31 summer measurements in the altitude range 40–60 km. Up to three wavelengths have been considered at each height.

4.2. Vertical Wavelengths

[21] The advantage of lidars covering a large altitude range is most relevant when determining vertical wavelengths. For example, in the center of our height range (~40–60 km) our technique allows to detect vertical wavelengths up to 50 km. In this height range we determine the most prominent wavelengths in every night analyzing the wavelet spectrum similar to the examples shown in Figures 4 and 6. As for these examples in most nights a significant part of the observed fluctuations (up to 45–65%) is given by up to three dominating waves. The distribution of these wavelengths in all nights is shown in Figure 8. All vertical wavelengths within our instrumental limit (5–50 km) have been detected, both in summer and winter. In both seasons smaller wavelengths (<22 km) are more frequent compared to larger wavelengths. We note that small vertical wavelengths are typical for internal gravity waves, whereas large wavelengths are caused by both internal gravity waves and tides. Interestingly, we observe gaps in the distributions around 22 km both in summer and winter. The gaps are not statistically significant because of the small number of measurements. It remains to be seen whether this phenomenon persists when more measurements are available. At the moment we cannot find any instrumental or technical reasons for these gaps. Since we find these gaps in both seasons we speculate that they are of still unexplained geophysical origin.

5. Discussion

5.1. Variability as Function of Altitude

[22] The magnitude of the temperature fluctuations generally increases with altitude and in some cases reaches ~20 K at mesopause altitudes. At lower heights the scale height of amplitude growth is approximately 18–22 km (= $2H_E$) which is substantially larger than expected from undisturbed gravity wave propagation ($2H_\rho$ = 14 km). This means that the amplitude of the observed fluctuations increases less with altitude than expected from undisturbed gravity wave propagation which has also been found by *Smith et al.* [1987] and *Wilson et al.* [1991b]. Adding to the results from the winter and summer examples we have studied the altitude-dependent growth of the fluctuations shown in Figure 7 more qualitatively. Therefore we identify height regions with "reduced growth" as follows: At every kilometer we "launch" an exponential function $A \exp(z/2H_\rho)$ where A is the mean fluctuation at that altitude and H_ρ = 7 km is the density scale height. The main results do not critically depend on the choice of $H_\rho = 7 \pm 2$ km. We then determine the altitude where this function exceeds the observed fluctuations given by the mean plus the standard deviation. Such a "damping layer" indicates that a significant part of wave energy has disappeared at or below this height. Note that the intensity of wave damping is only indirectly determined by this procedure. We then count how often such a damping layer occurs at each altitude. The results are shown in Figure 9. In winter and summer there are significant number of damping layers at about 46 km and 44 km, respectively. Although in summer this region is somewhat below the stratopause we suppose that changing static stability causes the increased filtering and breaking. In winter wave damping is observed nearly everywhere above 45 km, whereas in summer we find extended altitude regions (20–40 km and 76–89 km) with undisturbed gravity wave propagation. We note that a significant static instability region is present around the summer mesopause, i.e., where the temperature gradient changes dramatically. It is expected from theory that saturated gravity waves become unstable when they encounter drastic changes in static stability [*VanZandt and Fritts*, 1989].

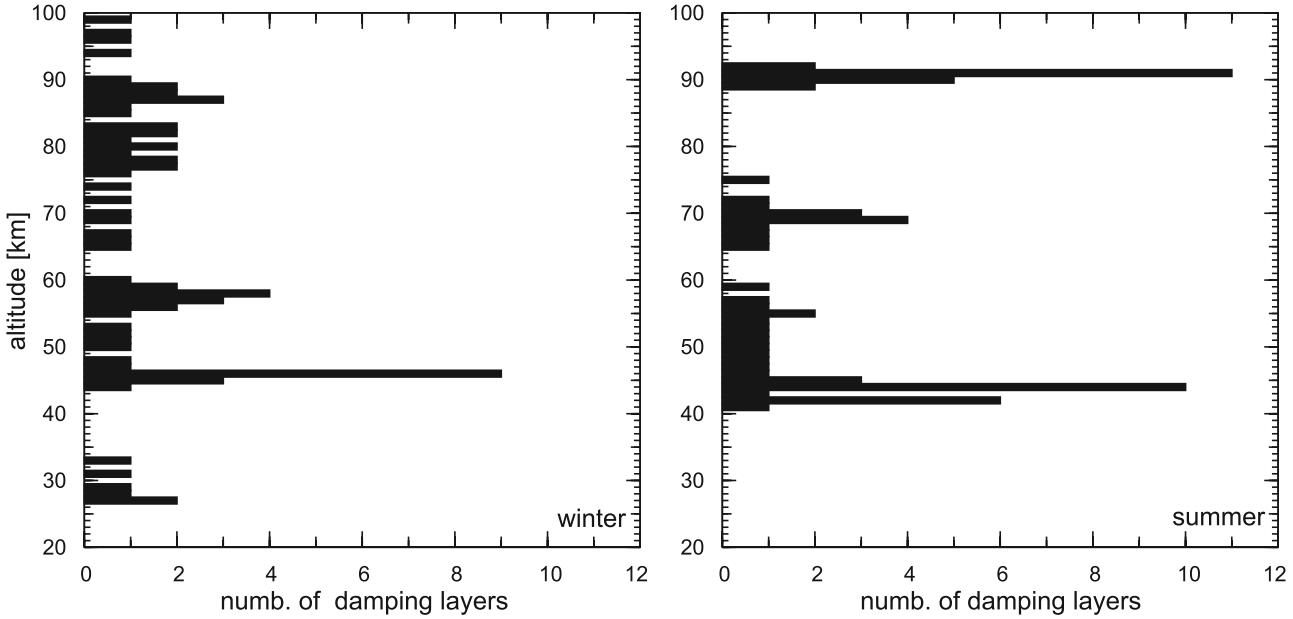

Figure 9. Altitude distribution of damping layers for (left) winter and (right) summer calculated from the red lines in Figure 7 (see text for details).

[23] We frequently observe height regions where the wave amplitudes are nearly constant with altitude or even decrease. Such "nodes" predominantly occur in the winter mesosphere (see section 3.1). Above these "nodes" the fluctuations increase again, limited by further breaking and reflection. After careful analysis we conclude that these "nodes" are not caused by our data sampling or processing techniques. We have therefore studied the background conditions in the vicinity of these "nodes." In about half of all cases we find very small Brunt-Väisälä frequencies ($N^2 < 10^{-4}s^{-2}$) at these altitudes. This suggests that convective instabilities are an important mechanism causing these "nodes." Strictly speaking small positive Brunt-Väisälä frequencies are still assumed to represent stable conditions. However, convective instabilities are expected only for few minutes [e.g., *Sica and Thorsley*, 1996; *Sherman and She*, 2006]. Because of our longer integration time of 1 hour convective instabilities are often smoothed out to small, but positives values of N^2. Therefore we use small N^2 numbers as an appropriate indicator for convective instabilities. Other damping mechanisms, such as dynamical instabilities or critical layer filtering may also cause drastic amplitude reduction.

[24] As noted before, we observe that the absolute value of vertical phase speed $c_{\phi,z}$ varies with altitude. In summer and winter $|c_{\phi,z}|$ is larger in the mesosphere than in the stratosphere. This increase of $c_{\phi,z}$ is expected from the variation of static stability with altitude. From the dispersion relation we get $c_{\phi,z} \propto \lambda_z \propto 1/N$ assuming that the wave period does not vary [*Fritts and Alexander*, 2003]. In the stratosphere N is larger compared to the mesosphere which results in smaller vertical wavelengths and smaller vertical phase speeds. Static stability also explains the seasonal variation of $c_{\phi,z}$: The absolute temperature lapse rate is larger in the summer mesosphere (compared to winter) which results in smaller Brunt-Väisälä frequencies and hence larger phase speeds.

5.2. Seasonal Variation of Fluctuations

[25] In our observations we find a strong seasonal variation of temperature fluctuations due to gravity waves. The fluctuations are about 2–4 times larger in winter compared to summer (altitude range: 40–90 km; see Table 1). This is in agreement with lidar measurements by *Wilson et al.* [1991b]. How much of this difference is due to the different length of the measurements, namely 12 hours in winter relative to 3.5 hours in summer? We have studied this effect on our examples presented earlier and have restricted the winter data to the local time period 2145–0115 UT, i.e., the same period as in summer. The corresponding mean deviations are in Table 1. Indeed, the 12-hour values are approximately 1.5 times larger than the 3.5-hour values. Still, the 3.5-hour values in winter are a factor of 1.5–2.5 larger than in summer (at least above 40 km, see Table 1). We conclude that the main reason for the winter/summer difference of temperature variability is of geophysical origin and that it is not caused by the different sampling periods. In section 4.1 and in the following discussion we use the 3–5 hour values for the entire set of measurements (winter and summer).

[26] Figure 10 presents the ratio of the mean fluctuations shown in Figure 7. The winter/summer ratio is in the entire altitude range (20–100 km) larger than 1 and reaches a maximum of about 2.5 in the mesosphere. To study this result more quantitatively we use a simplified polarization relation for temperature fluctuations of unsaturated gravity waves [see *Eckermann*, 1995, equation (21)]:

$$T'(z) \propto T_\circ(z) \cdot N(z)^{3/2} \cdot E(z) = T_\circ(z) \cdot N(z)^{3/2} \cdot \exp \int_{z_0}^{z} \frac{dz}{2H_\rho(z)} \quad (1)$$

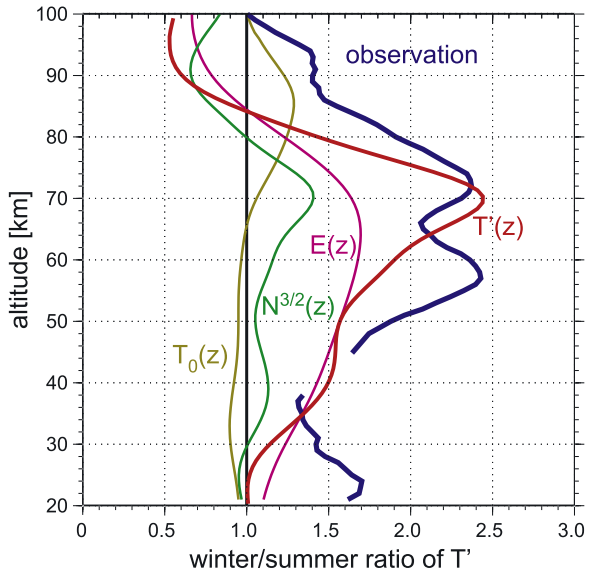

Figure 10. Observed winter/summer ratio of mean fluctuations (blue line) compared to the expected ratio from a simplified theory $T'(z)$ (red line). Mean lidar temperature profiles have been used to determine $T'(z)$. Various factors contributing to $T'(z)$ are shown as thin lines (see equation (1) and text for more details).

where $T'(z)$ is the temperature fluctuation, T_0 is the background temperature, N is the Brunt-Väisälä frequency, and $E(z) = \exp \int_{z_0}^{z} \frac{dz}{2H_\rho(z)}$ is the increase of amplitudes due to decreasing air density. As pointed out by *Eckermann* [1995], this approximation neglects the effect of background winds, the saturation of waves, and any potential differences in the gravity wave source. The winter/summer ratios from equation (1) are also shown in Figure 10. It is important to note that we have used mean temperature profiles from our actual measurements for this analysis rather than any reference atmosphere. The ratios of the individual terms shown in Figure 10 (thin lines) are therefore based on real measurements and not on empirical models.

[27] In general we find good agreement between equation (1) and our observations but also some systematic differences in the lower mesosphere and above 80 km. The good agreement between 60 and 80 km has also been observed by *Eckermann* [1995]. As can be seen in Figure 10 the main reasons for the winter/summer ratio comes from different exponential increase and the different Brunt-Väisälä frequencies, whereas mean temperatures play a minor role. The discrepancies between observations and equation (1) in the lower mesosphere and above 80 km suggest that the approximations used to derive equation (1) are not adequate here. For example, the complete polarization relation also depends on the background winds. Furthermore, we have already shown that wave amplitudes are damped. In Figure 9 we have shown that the preferred damping regions are different in summer and winter. In the upper stratosphere more filtering and damping takes place in summer than in winter (cf. Figure 9), which is in agreement with the smaller winter/summer ratio from the background temperatures compared to the observed ratio at about 55 km. Between 60–80 km the effect of filtering and damping on the amplitudes seems to be similar in both seasons, which produces a nearly constant winter/summer ratio. Above 80 km the influence of the summer mesopause as a particular region of enhanced gravity wave damping produces a larger observed ratio than expected from the background temperature alone. The saturation of waves also plays an important role.

[28] Can tides contribute to the summer/winter difference of temperature fluctuations? This is rather unlikely for the following reasons: Because of our data reduction procedure wave components with periods larger than the sampling period (for example diurnal tides) do not contribute to the fluctuations. From the potassium lidar (which is daylight capable but does not cover the entire mesosphere) we know that typical semidiurnal tidal amplitudes are in the range of 5–10 K at 89 km above our site [*Shepherd and Fricke-Begemann*, 2004; *Fricke-Begemann and Höffner*, 2005]. This is only about one third of the total observed fluctuations at this altitude. We conclude that tides play a minor role for the observed winter/summer ratio of mean fluctuations. A comprehensive tidal study requires daylight capability of the RMR lidar which is not yet available.

5.3. General Topics

[29] Gravity waves propagating in the atmosphere may encounter critical levels if the phase speed equals the mean background wind speed in the direction of wave propagation. We tried to find a systematic dependence of gravity wave fluctuations on background winds taken from ECMWF (European Centre for Medium-Range Weather Forecasts) close to Kühlungsborn. We have used mean winds and gravity wave fluctuations at various altitudes but could not identify any significant correlation between these quantities. There are several explanations for this lack of correlation. We do not know the horizontal path of the gravity waves and therefore cannot examine the wind regimes they have been exposed to. A further analysis requires detailed modeling applying ray tracing of gravity waves. Furthermore, a better understanding of the spatial and temporal distribution of sources is required for such an analysis. For example, gravity waves excited by orography have intrinsic phase velocities close to zero, whereas other sources support large phase velocities [e.g., *Alexander and Dunkerton*, 1999]. Presumably, these sources systematically depend on season at our side. A final interpretation of our results can therefore only be given with the help of sophisticated models of gravity wave generation, propagation, and dissipation. Despite these limitations our observations clearly demonstrate that filtering and damping of gravity waves takes place with significant seasonal differences.

[30] We may speculate that our measurements are somewhat biased because lidar measurements can only be performed during clear sky. This implies that we systematically lack sampling during bad weather conditions, e.g., when frontal systems pass our station and may locally generate gravity waves. We argue that such a local influence is rather unlikely since gravity waves travel from all sides into the lidar beam. Gravity waves observed in the stratosphere and mesosphere may have propagated several hundred kilometers horizontally from their sources. We

therefore do not expect a significant local influence on our observations. Even if such an influence should exist it will presumably not alter our results regarding summer/winter differences since the influence is most likely independent of season.

[31] Our results are compatible with former lidar observations, for example regarding the range of vertical phase speeds and the growth of amplitudes with altitude [*Chanin and Hauchecorne*, 1981; *Gardner et al.*, 1989; *Wilson et al.*, 1991b], as well as the fact that a significant part of total variability is given by only few dominating waves [*Sica and Russell*, 1999]. We note, however, that the possibility of intercomparisons is rather limited since most former measurements cover a smaller altitude range and/or are performed at other latitudes [*Chanin and Hauchecorne*, 1981; *Shibata et al.*, 1986; *Gardner et al.*, 1989; *Wilson et al.*, 1991b; *Sica and Russell*, 1999]. Therefore we hesitate to perform a detailed comparison of wave parameters with other measurements.

6. Conclusions and Outlook

[32] We have presented winter and summer measurements of temperature fluctuations from a combined system of lidar instruments which for the first time allows to measure thermal wave structures quasi-continuously from the troposphere up to the lower thermosphere. We have used all available nights for winter (14) and summer (31) with measurement durations per night of more than 3 hours.

[33] Our measurements show large temperature fluctuations (more than 20 K), particularly in the upper mesosphere in winter. These fluctuations often grow exponentially with altitude, however, at a rate which is generally slower than expected from undisturbed gravity wave propagation. This indicates that dissipation of gravity wave energy and/or filtering of waves takes place. We also find local height ranges (especially in the winter mesosphere) where the fluctuations are very small. These ''nodes'' are frequently associated with convective instabilities. However, we cannot exclude that other mechanisms, such as dynamical instabilities or critical filtering, may have contributed to the abrupt disappearance of wave fluctuations.

[34] In general, fluctuations are larger in winter than in summer in the entire altitude range (20–100 km) with the largest ratio of 2–2.5 in the mesosphere. We have analyzed this winter/summer differences using our lidar background temperatures and found that in the height range 60–80 km the ratio is nearly entirely due to the difference in Brunt-Väisälä frequency and air densities. At other altitudes, in particular in the lower mesosphere and around the mesopause, the ratio points to different filtering and damping in winter compared to summer. This is supported by the fact that the observed amplitude growth is less pronounced than expected for undisturbed and unsaturated wave propagation in both seasons. Despite of some altitude ranges with undisturbed propagation in summer, the upper stratosphere and the mesopause in summer are particular regions of enhanced and strong gravity wave damping.

[35] We have analyzed the fluctuations in terms of vertical wavelengths, periods, and phase speeds. In both seasons we find the entire range of wavelengths between approximately 5 and 50 km (large wavelengths may be influenced by tides), but small wavelengths (<22 km) are more frequent. In a single night a few waves dominate the fluctuations and contribute ~45–65% of the total variability. This experimental result constrains model simulations of gravity wave generation, propagation, and dissipation. In general, our observed wave parameters are in the range of previous lidar observations, ($c_{\phi,z} = -0.25$ to -1.9 m/s, $P = 1$ to 8 hours, λ_z = 10 to 20 km). However, we also find significant differences, for example regarding dominating waves with $\lambda_z > 25$ km.

[36] The lidar technique covers a large altitude range for gravity wave studies, namely from just above the source region (troposphere/lower stratosphere) to the upper atmosphere where propagation, filtering, and dissipation occurs. We have shown that the large height range and the high spatial and temporal resolution allow study of an important part of the gravity wave spectrum, namely the low- and medium-frequency waves. A limitation comes from the fact that measurements are taken at one location only. We therefore do not know whether the observed gravity waves are generated locally or propagate horizontally into our lidar beam. A network of lidars could improve this deficiency.

[37] In future we will continue our measurements to also cover spring and autumn and to study intra-annual variations. We will also extend our data interpretation by including supporting information, for example winds from radars or from ECMWF. We also plan to compare our results with theoretical simulations of gravity wave generation, propagation, and dissipation and with gravity wave parameterizations used in global circulation models.

[38] **Acknowledgments.** We thank Matthias Alpers (now at DLR Bonn) for developing the IAP RMR lidar until autumn 2002 and Torsten Köpnick for designing electronics for all IAP lidars. For valuable discussions on gravity wave analyses we thank C. Fricke-Begemann. The large number of lidar soundings would not be possible without our colleagues at IAP. We are grateful to the anonymous reviewers for their helpful questions and recommendations. This research is supported by the Deutsche Forschungsgemeinschaft (DFG) under grant GE 1625/1-1.

References

Alexander, M. J., and T. J. Dunkerton (1999), A spectral parameterization of mean-flow forcing due to breaking gravity waves, *J. Atmos. Sci.*, *56*(24), 4167–4182, doi:10.1175/1520-0469(1999)056<4167:ASPOMF>2.0.CO;2.

Allen, S. J., and R. A. Vincent (1995), Gravity wave activity in the lower atmosphere: Seasonal and latitudinal variations, *J. Geophys. Res.*, *100*(D1), 1327–1350.

Alpers, M., R. Eixmann, C. Fricke-Begemann, M. Gerding, and J. Höffner (2004), Temperature lidar measurements from 1 to 105 km altitude using resonance, Rayleigh, and rotational Raman scattering, *Atmos. Chem. Phys.*, *4*, 793–800.

Chanin, M.-L., and A. Hauchecorne (1981), Lidar observations of gravity and tidal waves in the stratosphere and mesosphere, *J. Geophys. Res.*, *86*(C10), 9715–9721.

Dalin, P., S. Kirkwood, A. Moström, K. Stebel, P. Hoffmann, and W. Singer (2004), A case study of gravity waves in noctilucent clouds, *Ann. Geophys.*, *22*, 1875–1884.

Dao, P. D., R. Farely, X. Tao, and C. S. Gardner (1995), Lidar observations of the temperature profile between 25 and 105 km: Evidence of strong tidal perturbations, *Geophys. Res. Lett.*, *22*(20), 2825–2828.

Dörnbrack, A., T. Birner, A. Fix, H. Flentje, A. Meister, H. Schmid, E. V. Browell, and M. J. Mahoney (2002), Evidence for inertia gravity waves forming polar stratospheric clouds over Scandinavia, *J. Geophys. Res.*, *107*(D20), 8287, doi:10.1029/2001JD000452.

Eckermann, S. D. (1995), On the observed morphology of gravity-wave and equatorial-wave variance in the stratosphere, *J. Atmos. Terr. Phys.*, *57*(2), 105–134, doi:10.1016/0021-9169(93)E0027-7.

Eckermann, S. D., I. Hirota, and W. K. Hocking (1995), Gravity wave and equatorial wave morphology of the stratosphere derived from long-term

rocket soundings, *Q. J. R. Meteorol. Soc.*, *121*(521), 149–186, doi:10.1256/smsqj.52107.
Ern, M., P. Preusse, M. J. Alexander, and C. D. Warner (2004), Absolute values of gravity wave momentum flux derived from satellite data, *J. Geophys. Res.*, *109*, D20103, doi:10.1029/2004JD004752.
Fetzer, E. J., and J. C. Gille (1994), Gravity wave variance in LIMS temperatures, part 1, Variability and comparison with backround winds, *J. Atmos. Sci.*, *51*(17), 2461–2483, doi:10.1175/1520-0469(1994)051<2461:GWVILT>2.0.CO;2.
Fleming, E. L., S. Chandra, J. J. Barnett, and M. Corney (1990), Zonal mean temperature, pressure, zonal wind, and geopotential height as functions of latitude, COSPAR international reference atmosphere: 1986, part II: Middle atmosphere models, *Adv. Space Res.*, *10*(12), 11–59, doi:10.1016/0273-1177(90)90386-E.
Fricke-Begemann, C., and J. Höffner (2005), Temperature tides and waves near the mesopause from lidar observations at two latitudes, *J. Geophys. Res.*, *110*, D19103, doi:10.1029/2005JD005770.
Fricke-Begemann, C., M. Alpers, and J. Höffner (2002), Daylight rejection with a new receiver for potassium resonance temperature lidars, *Opt. Lett.*, *27*(21), 1932–1934.
Fritts, D. C., and M. J. Alexander (2003), Gravity wave dynamics and effects in the middle atmosphere, *Rev. Geophys.*, *41*(1), 1003, doi:10.1029/2001RG000106.
Gardner, C. S., and D. G. Voelz (1987), Lidar studies of the nighttime sodium layer over Urbana, Illinois: 2. Gravity waves, *J. Geophys. Res.*, *92*(A5), 4673–4694.
Gardner, C. S., M. S. Miller, and C. H. Liu (1989), Rayleigh lidar observations of gravity wave activity in the upper stratosphere at Urbana, Illinois, *J. Atmos. Sci.*, *46*(12), 1838–1854, doi:10.1175/1520-0469(1989)046<1838:RLOOGW>2.0.CO;2.
Gerding, M., M. Rauthe, and J. Höffner (2004), Temperature soundings from 1 to 105 km altitude by combination of co-located lidars, and its application for gravity wave examination, in *Reviewed and Revised Papers Presented at the 22nd International Laser Radar Conference*, edited by G. Pappalardo and A. Amodeo, *Eur. Space Agency Spec. Pap. ESA SP-561*, 567–570.
Hecht, J. H., S. Kovalam, P. T. May, G. Mills, R. A. Vincent, R. L. Walterscheid, and J. Woithe (2004), Airglow imager observations of atmospheric gravity waves at Alice Springs and Adelaide, Australia during the Darwin Area Wave Experiment (DAWEX), *J. Geophys. Res.*, *109*, D20S05, doi:10.1029/2004JD004697.
Hertzog, A., F. Vial, A. Dörnbrack, S. D. Eckermann, B. M. Knudsen, and J.-P. Pommereau (2002), In situ observations of gravity waves and comparisons with numerical simulations during the SOLVE/THESEO 2000 campaign, *J. Geophys. Res.*, *107*(D20), 8292, doi:10.1029/2001JD001025.
Holton, J. R. (1982), The role of gravity wave induced drag and diffusion in the momentum budget of the mesosphere, *J. Atmos. Sci.*, *39*(4), 791–799, doi:10.1175/1520-0469(1982)039<0791:TROGWI>2.0.CO;2.
Holton, J. R., and M. J. Alexander (2000), The role of waves in the transport circulation of the middle atmosphere, in *Atmospheric Science Across the Stratopause*, *AGU Monogr. Ser.*, vol. 123, edited by D. E. Siskind, S. D. Eckermann, and M. E. Summers, pp. 21–35, AGU, Washington D. C.
Lindzen, R. S. (1981), Turbulence and stress owing to gravity wave and tidal breakdown, *J. Geophys. Res.*, *86*(C10), 9707–9714.
Manzini, E., and N. A. McFarlane (1998), The effect of varying the source spectrum of a gravity wave parameterization in middle atmosphere general circulation model, *J. Geophys. Res.*, *103*(D24), 31,523–31,539.
Meek, C. E., I. M. Reid, and A. Manson (1985), Observations of mesospheric wind velocities: 2. Cross sections of power spectral densities for 48–8 hours, 8–1 hours, and 1 hour to 10 min over 60–110 km for 1981, *Radio Sci.*, *20*(6), 1383–1402.
Nakamura, T., T. Tsuda, S. Fukao, A. H. Manson, C. E. Meek, R. A. Vincent, and I. M. Reid (1996), Mesospheric gravity waves at Saskatoon (52°N), Kyoto (35°N), and Adelaide (35°S), *J. Geophys. Res.*, *101*(D3), 7005–7012.
Preusse, P., A. Dörnbrack, S. D. Eckermann, M. Riese, B. Schaeler, J. T. Bacmeister, D. Broutman, and K. U. Grossmann (2002), Space-based measurements of stratospheric mountain waves by CRISTA: 1. Sensitivity, analysis method, and a case study, *J. Geophys. Res.*, *107*(D23), 8178, doi:10.1029/2001JD000699.
Rapp, M., B. Strelnikov, A. Müllemann, F.-J. Lübken, and D. C. Fritts (2004), Turbulence measurements and implications for gravity wave dissipation during the MaCWAVE/MIDAS rocket program, *Geophys. Res. Lett.*, *31*, L24S07, doi:10.1029/2003GL019325.
Schöch, A., G. Baumgarten, D. C. Fritts, P. Hoffmann, A. Serafimovich, L. Wang, P. Dalin, A. Müllemann, and F. J. Schmidlin (2004), Gravity waves in the troposphere and stratosphere during the MaCWAVE/MIDAS summer rocket program, *Geophys. Res. Lett.*, *31*, L24S04, doi:10.1029/2004GL019837.
Serafimovich, A., P. Hoffmann, D. Peters, and V. Lehmann (2005), Investigation of inertia-gravity waves in the upper troposphere/lower stratosphere over northern Germany observed with collocated VHF/UHF radars, *Atmos. Chem. Phys.*, *5*(2), 295–310.
Shepherd, M., and C. Fricke-Begemann (2004), Study of tidal variations in mesospheric temperature at low and mid latitudes from WINDII and potassium lidar observations, *Ann. Geophys.*, *22*(4), 1513–1528.
Sherman, J. P., and C.-Y. She (2006), Seasonal variation of mesopause region wind shears, convective and dynamic instabilities above Fort Collins, CO: A statistical study, *J. Atmos. Sol. Terr. Phys.*, *68*(10), 1061–1074.
Shibata, T., M. Kobuchi, and M. Maeda (1986), Measurements of density and temperature profiles in the middle atmosphere with a XeF lidar, *Appl. Opt.*, *25*(5), 685–688.
Sica, R. J., and A. Russell (1999), How many waves are in the gravity wave spectrum?, *Geophys. Res. Lett.*, *26*(24), 3617–3620.
Sica, R. J., and M. D. Thorsley (1996), Measurements of superadiabatic lapse rates in the middle atmosphere, *Geophys. Res. Lett.*, *23*(20), 2797–2800.
Sica, R. J., S. Sargoytchev, P. S. Argall, E. F. Borra, and L. Girard (1995), Lidar measurements taken with a large-aperture liquid mirror: 1. Rayleigh-scatter system, *Appl. Opt.*, *34*(30), 6925–6936.
Smith, S. A., D. C. Fritts, and T. E. VanZandt (1987), Evidence for a saturated spectrum of atmospheric gravity waves, *J. Atmos. Sci.*, *44*(10), 1404–1410, doi:10.1175/1520-0469(1987)044<1404:EFASSO>2.0.CO;2.
Torrence, C., and G. P. Compo (1998), A practical guide to wavelet analysis, *Bull. Am. Meteorol. Soc.*, *79*(1), 61–78, doi:10.1175/1520-0477(1998)079<0061:APGTWA>2.0.CO;2.
VanZandt, T. E., and D. C. Fritts (1989), A theory of enhanced saturation of the gravity wave spectrum due to increases in atmospheric stability, *Pure Appl. Geophys.*, *130*(2–3), 399–420, doi:10.1007/BF00874466.
Vaughan, G., D. P. Wareing, S. J. Pepler, L. Thomas, and V. M. Mitev (1993), Atmospheric temperature measurements made by rotational Raman scattering, *Appl. Opt.*, *32*(15), 2758–2764.
Vincent, R. A., and M. J. Alexander (2000), Gravity waves in the tropical lower stratosphere: An observational study of seasonal and annual variability, *J. Geophys. Res.*, *105*(D14), 17,971–17,982.
von Zahn, U., and J. Höffner (1996), Mesopause temperature profiling by potassium lidar, *Geophys. Res. Lett.*, *23*(2), 141–144.
Williams, B. P., D. C. Fritts, L. Wang, C. Y. She, J. D. Vance, F. J. Schmidlin, R. A. Goldberg, A. Müllemann, and F.-J. Lübken (2004), Gravity waves in the arctic mesosphere during the MaCWAVE/MIDAS summer rocket program, *Geophys. Res. Lett.*, *31*, L24S05, doi:10.1029/2004GL020049.
Wilson, R., M. L. Chanin, and A. Hauchecorne (1991a), Gravity waves in the middle atmosphere observed by Rayleigh lidar: 1. Case studies, *J. Geophys. Res.*, *96*(D3), 5153–5167.
Wilson, R., M. L. Chanin, and A. Hauchecorne (1991b), Gravity waves in the middle atmosphere observed by Rayleigh lidar: 2. Climatology, *J. Geophys. Res.*, *96*(D3), 5169–5183.

M. Gerding, J. Höffner, F.-J. Lübken, and M. Rauthe, Leibniz-Institut für Atmosphärenphysik an der Universität Rostock, Schloss-Straße 6, D-18225 Kühlungsborn, Germany. (rauthe@iap-kborn.de)